



Laminar burning velocities at high pressure for primary reference fuels and gasoline: Experimental and numerical investigation

S. Jerzembeck^{a,*}, N. Peters^a, P. Pepiot-Desjardins^b, H. Pitsch^b

^a RWTH, Aachen, Germany

^b Department of Mechanical Engineering, Stanford University, CA, USA

ARTICLE INFO

Article history:

Received 19 November 2007

Received in revised form 31 May 2008

Accepted 4 November 2008

Available online 6 December 2008

Keywords:

Gasoline

Primary reference fuels

Laminar burning velocities

Reduced kinetic mechanisms

ABSTRACT

Spherical flames of *n*-heptane, iso-octane, PRF 87 and gasoline/air mixtures are experimentally investigated to determine laminar burning velocities and Markstein lengths under engine-relevant conditions by using the constant volume bomb method. Data are obtained for an initial temperature of 373 K, equivalence ratios varying from $\phi = 0.7$ to $\phi = 1.2$, and initial pressures from 10 to 25 bar. To track the flame front in the vessel a dark field He–Ne laser Schlieren measurement technique and digital image processing were used. The propagating speed with respect to the burned gases and the stretch rate are determined from the rate of change of the flame radius. The laminar burning velocities are obtained through a linear extrapolation to zero stretch. The experimentally determined Markstein numbers are compared to theoretical predictions. A reduced chemical kinetic mechanism for *n*-heptane and iso-octane was derived from the Lawrence Livermore comprehensive mechanisms. This mechanism was validated for ignition delay times and flame propagation at low and high pressures. In summary an overall good agreement with the various experimental data sets used in the validation was obtained.

© 2008 The Combustion Institute. Published by Elsevier Inc. All rights reserved.

1. Introduction

In recent years, improving fuel economy and reducing pollutant emissions of engines have become the focus of a considerable amount of research. For gasoline internal combustion engines, two different combustion technologies can be identified. The first one is the conventional Spark Ignition (SI) engine, in which a mixture of fuel and air is ignited by a spark and combustion proceeds by flame propagation through the cylinder. A thorough understanding of the transition from laminar to turbulent flame kernel and to turbulent flame propagation is essential for designing more efficient engines, and it has been shown that the laminar burning velocity is a key parameter for these phenomena [1–3]. Also, auto-ignition of the mixture in an SI engine, relevant for engine knock, is a highly undesirable event that restricts the maximum operating compression ratio, and ultimately, the thermodynamic efficiency of the engine. The second technology is the relatively new homogeneous-charge compression ignition (HCCI) concept. HCCI engines are of particular interest because of their potential to reduce NO_x and soot emissions and their higher thermal efficiency compared to SI engines. The performance of an HCCI engine relies on an accurate control of the auto-ignition timing of the mixture. Recent work has shown that charge stratification may be such that both auto-

ignition and flame propagation can coexist during the combustion process [4]. Simulating HCCI combustion chemistry therefore requires the ability to accurately predict the auto-ignition behavior of the fuel at high pressures and low temperatures, along with the accurate prediction of flame propagation. Thus, a precise description of the chemical phenomena occurring in both homogeneous combustion and flame configurations is essential in the simulation of an internal combustion engine, either SI or HCCI.

Chemical modeling starts with a correct representation of the real fuel of interest. Gasoline is a mixture of hundreds of different chemical compounds. Deriving a detailed chemical model for gasoline is therefore impossible, and the fuel representation needs to be simplified drastically to be included in numerical simulations. The first level of simplification consists in approximating the fuel by a well-defined mixture of a few components that will match some physical or chemical properties of the real fuel, such as hydrogen-to-carbon ratio, density or boiling characteristics. Using surrogate fuels in lieu of real fuels presents numerous advantages, among which are the reproducibility of experiments and the possibility of formulating chemical models suitable for CFD. Recent progress in formulating appropriate gasoline surrogate compositions has been made in [5], for example. In the present work, the primary reference fuels, *n*-heptane and iso-octane, will be used as surrogate components.

Many studies, both experimental and numerical, have been conducted to characterize the auto-ignition and flame propagation characteristics of both *n*-heptane and iso-octane. Auto-ignition of

* Corresponding author.

E-mail address: sven.jerzembeck@rwth-aachen.de (S. Jerzembeck).

n-heptane has been studied in shock tube [6,7] and rapid compression machine [8] experiments, while auto-ignition characteristics of iso-octane and PRF mixtures at elevated pressures have been determined in [9–11]. Ignition delay times for gasoline have been measured mostly at elevated pressures in [11]. Laminar burning velocities of *n*-heptane, iso-octane and various PRF mixtures have been measured at atmospheric pressure [12–14]. Bradley et al. [15] reported laminar burning velocities and Markstein lengths for iso-octane/air and *n*-heptane/iso-octane/air mixtures up to 10 atm. A few other studies have considered high pressure flame propagation of iso-octane, such as the work of Metghalchi and Keck [16], in which data at high pressure were extrapolated from low pressure measurements, or the prior work of Gülder [17]. However, published data remain scarce and are not always consistent with one another.

On the modeling side, comprehensive chemical mechanisms have been developed for *n*-heptane [18], iso-octane [19] and mixtures of both [20]. These detailed mechanisms have been validated over a wide range of pressures, temperatures, and equivalence ratios in homogeneous configurations. However, their extremely large sizes prevent them from being validated for flame propagation. Recently, Chaos et al. [21] developed a short chemical mechanism to describe the high temperature oxidation and pyrolysis of *n*-heptane, iso-octane, and their mixtures. This mechanism was validated against experimental data for *n*-heptane and iso-octane shock tube ignition delay times, laminar burning velocities at atmospheric pressure and flow and jet-stirred reactors. Only temperatures above 950 K were considered. To model HCCI combustion, however, low temperature auto-ignition and the negative temperature coefficient (NTC) behavior are essential. The low temperature chemistry largely differs from what takes place at high temperature and involves a large number of additional species.

The objectives of this work are twofold. First, measurements of high pressure laminar burning velocities for primary reference fuels and standard commercial gasoline are obtained to complement the experimental data available in the literature. Then, a short kinetic mechanism, able to correctly represent both low and high temperature chemistry in homogeneous configurations and flame propagation, is derived from the LLNL detailed mechanisms for *n*-heptane and iso-octane. The data obtained in the experimental part are used to validate the mechanism at high pressures. An electronic version of the short kinetic mechanisms and the thermodynamic and transport data used in the paper can be downloaded online [22].

2. Experimental technique

Fig. 1 illustrates the experimental setup that was used for all experiments. The setup consists of an enclosed pressure vessel providing optical access through two windows with a diameter of 50 mm, positioned on opposite sides of the 100 mm diameter vessel. The pressure vessel was designed for static pressures up to 400 bar, as were all devices connected to it. To ensure complete evaporation of the fuels, the vessel was heated to 160 °C by four symmetrically arranged heat cartridges (200 W each), whereof two were fully inserted into two closed tubes positioned in the combustion chamber of the vessel. Those two heat cartridges generated a temperature of approximately 180 °C, which, as a result of the thus induced temperature differences inside the vessel, evoked natural convection to stir the mixture. After a few minutes the heat cartridges were turned off. The heat dissipation decelerated the motion of the gas and finally it stalled at a uniformly distributed temperature of 100 °C. To preserve the temperature of the heat cartridges, four PID-controllers with four K-type thermocouples were applied, two K-type thermocouples (1 mm in diameter) were used to measure the gas temperature inside the vessel. Reaching the

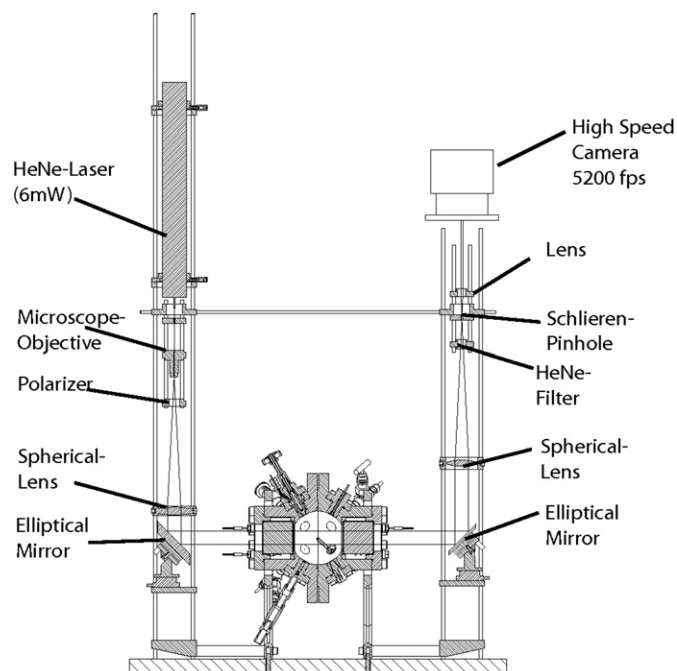


Fig. 1. Optical Schlieren measurement setup and closed pressure vessel.

mark of 100 °C, the mixture then was ignited from the middle of the vessel using a slightly modified standard ignition plug from BERU. The electrodes of the ignition plug (1 mm in diameter) had been modified so that both of their ends were positioned in the middle of the vessel. Furthermore, a two-step ignition system was developed for sparking to provide minimum ignition energy to the mixture. This ignition system generated a spark with duration of 1 ms. Firstly, as the vessel was being heated up, the necessary amount of fuel was determined, and by using a syringe system, injected into the vessel. Considering the correct increase of pressure change caused by the evaporation of the liquid fuel compared to the thermodynamic real-gas law calculations, air was being filled in very slowly (approx. isothermally) through a very fine needle valve, using two pressure transducers (type: Kistler 4075 A20 and A100) to control the filling process. An absolute pressure signal was obtained. The pressure rise during the combustion processes was determined by a Kistler 4075 A500 transducer. During combustion, the measured pressure increase of the unburned mixture was below 1.6 percent of the initial pressure before the expanded flame reached the circular window border. An asymptotic analysis [23] predicts that such a pressure increase may change the laminar flame velocity by less than one percent. Therefore, this effect has been neglected. The filling process itself took between 5 and 15 min, depending on the initial pressure of the mixture. After the filling process was completed, the two heat cartridges that had been employed to ensure a homogeneous mixture were turned back on for approximately 20 min. To track the flame, an optically Schlieren technique was applied, and a compact 10 mW Spectra Physics He–Ne laser ($\lambda = 632.8$ nm) was used as a light source with a beam diameter of 0.65 mm. The laser beam then was widened by a microscope lens (1:40), parallelized by a spherical biconvex lens (focal length $f = 300$ mm), and perpendicularly reflected by an elliptical mirror to the window through the vessel. Another elliptical mirror reflected the four beams to a spherical biconvex lens ($f = 200$ mm). In the focal point of this lens, a Schlieren pinhole of 0.6 mm in diameter filled its position. Additionally, a He–Ne filter ($\lambda = 632.8$ nm) was placed behind this optical device to prevent the CCD sensor from being overexposed by the radiation of the combustion process. A spherical achromatic

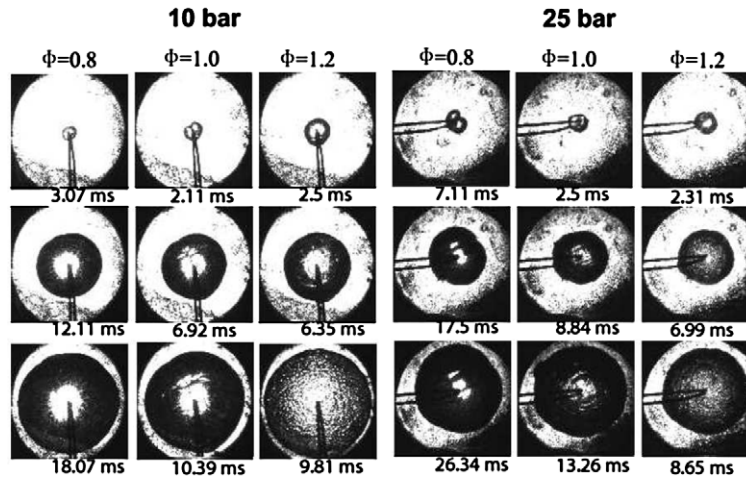


Fig. 2. Schlieren photographs of *n*-heptane/air mixtures, initial pressures are 10 and 25 bar, initial temperature is 373 K, equivalence ratios are 0.8, 1.0, and 1.2.

lens ($f = 80$ mm) parallelized the beam, and a Balsa 500 high speed camera with 5200 fps recorded the flame photographs. The resolution of the captured photographs amounted 100×100 pixels to map a region of approximately 25×25 mm². For each investigated fuel/air mixture, this cycle was carried out three times and the average value is reported.

3. Flame analysis

The experimental procedure used in this work follows closely that of Bradley et al. [15], Metghalchi and Keck [16], Law et al. [24], and Gülder [17]. These groups also investigated spherical expanding flames at high pressures to determine laminar burning velocities of premixed mixtures in a preheated closed vessel with optical access. In these works, data measured over a similar range of stretch rates were extrapolated to zero stretch value following the approach described below. Here, measurements were restricted to spherical, smooth flames with diameters above 5 mm to avoid spark influences. The flames were analyzed up to a diameter of 45–50 mm. It is known from the theory of laminar spherical flames that burned gas is motionless for the outward propagating flame [24,25]. The flame surface was tracked with an image processing code. A circle with the same area for each captured image was generated. The radii parameterized over time of these circles were used to determine the laminar burning velocity as a representative information of the expanding flame. Using the radii obtained from the captured flame images, the flame speed was determined by

$$S_b = \frac{dr_b}{dt}, \quad (1)$$

where S_b is the flame speed with respect to the burned gas and r_b is the flame front displacement. Therefore, values of the Schlieren radius r_{sch} , determined by image tracking of Schlieren cinematography, are close to r_b . Flame images were analyzed with an image processing code specifically developed for the experimental configuration to track flame front radii over time. The burned propagating flame speed S_b^0 was determined from first-order least squares fits through four radii adjacent to each point under consideration [15]. Contrast levels were set to define consistently flame fronts at all times.

Accounting for the effect of stretch, the burned gas unstretched flame speed S_b^0 was determined according to the relation [15,24,26,27]

$$S_b = S_b^0 - \mathcal{L}_b \kappa, \quad (2)$$

where \mathcal{L}_b is the burned Markstein length and κ is the stretch rate. The flame stretch rate κ at any point of the flame surface is defined as the Lagrangian time derivative of the logarithm of area A , an infinitesimal element of the surface surrounding the point [28]. For spherical flames, it has hence been defined as

$$\kappa = \frac{1}{A} \frac{dA}{dt} = \frac{2}{r_b} \frac{dr_b}{dt} \approx \frac{2}{r_{sch}} \frac{dr_{sch}}{dt} = \frac{2}{r_{sch}} S_b, \quad (3)$$

where A is the flame front surface area. Thus, by measuring the flame radius r_b versus time, \mathcal{L}_b and S_b^0 were obtained by a linear extrapolation to zero stretch [15]. The unburned unstretched flame speed (S_u^0) was obtained from continuity

$$S_b^0 \rho_b^0 = S_u^0 \rho_u. \quad (4)$$

The values ρ_b^0 and ρ_u are the burned and unburned densities of the mixture and were computed with the one dimensional flame code FlameMaster [29] and the mechanism derived below.

3.1. Stretch effects

Fig. 2 shows captured Schlieren photographs of *n*-heptane/air flames at 10 bar and 25 bar initial pressure for equivalence ratios 0.8, 1.0, and 1.2. The lean and the stoichiometric flames propagate smoothly and no wrinkles due to instability effects can be observed. However, for the rich case, the flames propagate smoothly shortly after sparking but onset of cellularity in the flame surface can be observed later on. The development of wrinkles corresponds to a sudden increase of propagating speed. Therefore, only information of smooth flames was used for flame analysis to determine laminar burning velocities as well as Markstein lengths.

Radiative heat losses can affect the propagation of expanding flames and therefore distort the accuracy of the determined laminar burning velocities. However, radiative heat losses affect the expanding flame only when the burning velocity is very low. Ronney [30] performed a time scale analysis on that phenomenon for spherical expanding flames. He discovered that this effect takes place for mixtures close to the flammability limits. In the present work, only mixtures close to stoichiometric conditions were investigated. Fig. 3 shows the curves for the propagating flame speed over stretch rate for different investigated fuel/air mixtures, initial pressures and equivalence ratios 0.8 and 1.2. Some scatter appears in the data in Fig. 3 for large stretch rates. This is due to differentiation of the raw data, which are affected by hydrodynamical instabilities. This scatter is much reduced at later times when the stretch rate decreases. The scatter introduced by hydrodynamical instabilities is unavoidable. Fig. 4 compares the evolution of the

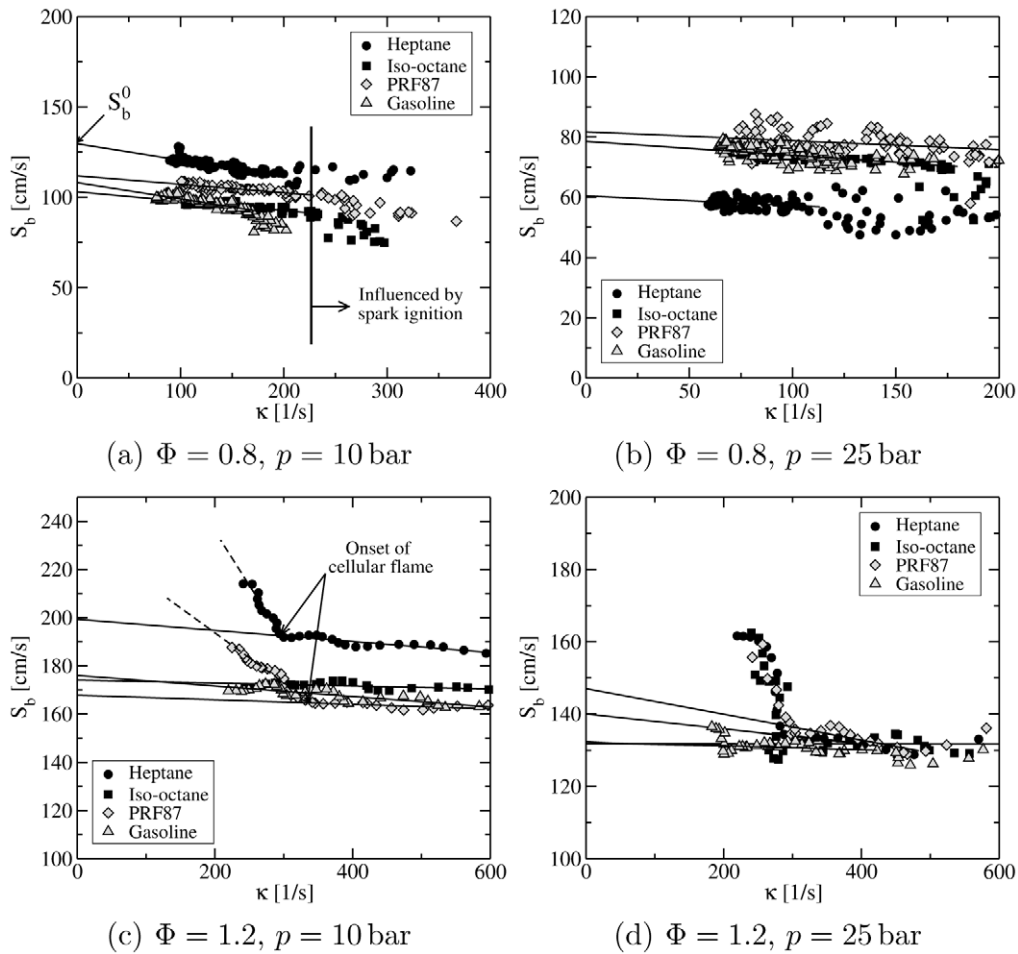


Fig. 3. Propagation speed over stretch rate for fuel/air ($X_{O_2}^{air} = 0.205$) mixtures for various pressures and equivalence ratios. S_b^0 is the flame speed with respect to the burned extrapolated to zero stretch.

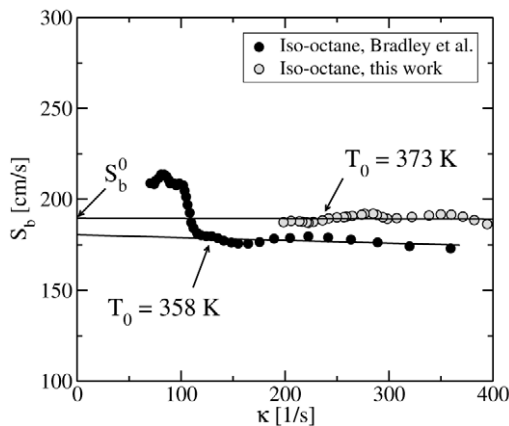


Fig. 4. Comparison of the propagation speed as a function of stretch between experimental data from Bradley et al. [15] and this work, for a stoichiometric mixture of iso-octane and air at an initial pressure of 10 bar.

laminar burning velocity as function of the stretch rate obtained for a stoichiometric mixture of iso-octane and air at $T_0 = 373$ K and 10 bar with that obtained by Bradley et al. [15] for the same mixture, but slightly lower temperature. Both results are in good qualitative and quantitative agreement, and illustrate the large sensitivity of laminar burning velocity on the temperature.

The Markstein length \mathcal{L}_b with respect to the burned mixture is expressed in dimensionless form as the Markstein number Ma_b

by normalizing it with the laminar flame thickness δ_l . Following Peters [25], δ_l can be defined for premixed flames as

$$\delta_l = \frac{(\lambda/c_p)_0}{(\rho_u S_u^0)}, \quad (5)$$

where the heat conductivity λ and the heat capacity c_p are evaluated at the inner layer temperature. These quantities and the unstretched laminar burning velocity S_u^0 appearing in this definition are determined for each mixture using one-dimensional flame calculations.

For each investigated fuel/air mixture, the Markstein length was determined as the negative slope of the best linear least squares fit through the measured values. The unstretched flame velocity S_b^0 was determined by linear extrapolation of smooth unwrinkled flame data to zero stretch, as shown by the fitted curves. At small stretch rates, the propagation speed of the expanding flame suddenly increases, as can be seen for example for the rich *n*-heptane flame. This increase in propagation speed resulted from the development of combustion instabilities that wrinkle the flame surface. It must be noted here that only data corresponding to smoothly expanding flames, before the onset of these instabilities, were considered to determine the laminar burning velocity at zero stretch. Fig. 3 illustrates the extrapolation procedure that was used.

The sharp increase of propagating speed caused by the onset of cellular flame enhancement at low stretch values was larger for the high pressure case (25 bar) than for the low pressure case (10 bar), due to the influence of initial mixture pressure. In agreement with the thermodiffusive stability theory, a larger positive

Markstein length was detected for lean “heavy” hydrocarbon/air mixtures and no onset of cellular flame development could be observed.

4. Mechanism development

The aim of this part is the development of a short chemical kinetic mechanism that can be used to simulate the new high pressure data for the laminar burning velocities of *n*-heptane, iso-octane, as well as mixtures of both. Essential prerequisites include the capability to simulate laminar burning velocities of those fuels and shorter alkanes such as methane, ethane, propane, butane, and iso-butane at low pressure. Additionally, as mentioned above, the correct prediction of auto-ignition of the primary reference fuels at all temperatures is necessary. The following sets of experimental data were used for the validation of the mechanism: shock tube ignition delay times for *n*-heptane [6–8] and iso-octane [9,11]/air mixtures, with pressures ranging from 1 to 40 bar, equivalence ratios between 0.5 and 2, and temperatures between 600 and 1500 K, laminar burning velocities at atmospheric pressure for methane [31–33], ethane [33–35], propane [33,35], butane and iso-butane [12], heptane, iso-octane, and PRF [12–14], laminar burning velocities at 5 atm for ethane and propane [35], and the new data for burning velocities at high pressure obtained as part of this work. As mentioned above as well, the comprehensive mechanisms for *n*-heptane [18] and iso-octane [19] auto-ignition from LLNL are used as starting schemes. This choice is motivated by the fact that these mechanisms are among the most comprehensive schemes existing in the literature.

Both starting mechanisms include hundreds of species and thousands of reactions. Such large sizes are unpractical for computing one-dimensional propagating flames and, therefore, smaller schemes have to be developed. The Directed Relation Graph with Error Propagation method (DRGEP) [36] has been used as an automatic reduction strategy to reduce the original mechanisms to a skeletal size. The DRGEP method aims to remove from the mechanism any species or reaction having a negligible effect on the prediction of a user-defined set of targets, such as ignition delay time or fuel consumption rate. To identify the unnecessary chemical pathways, the algorithm uses an error propagation strategy that estimates *a priori* the error introduced in a target when a group of species or reactions is removed from the mechanism. The reduction has been performed for auto-ignition over a chemical domain covering pressures from 1 to 40 atm, equivalence ratios from 0.5 to 2, and temperatures from 600 to 1500 K. The temperature range ensures that both high and low temperature chemistry, which are extremely different in the case of large molecules such as *n*-heptane and iso-octane, are retained in the skeletal mechanism. Indeed, at high temperature, oxidation proceeds through direct decomposition of the fuel radicals to smaller species, whereas at low temperature, molecular oxygen addition on fuel radicals are favored, and the reaction pathway proceeds through oxygenated species such as ketohydroperoxides, leading to complex two-stage ignition and negative temperature coefficient behavior [18]. The major assumptions made at that point are that the detailed mechanisms already include the correct chemical paths for propagating flames, and that this first reduction step does not remove any reactions significant for laminar flames. The latter assumption was verified for fuels up to butane by removing all species with more than four carbon atoms from the detailed LLNL mechanisms. These sub-mechanisms, including only about 200 species, were small enough to be used in 1D calculations. No significant differences, both in laminar burning velocity predictions and in the chemical structure of the flame, were found when comparing them to the skeletal mechanisms for auto-ignition, demonstrating that no major chemical paths in flames were removed from the detailed mechanism.

Moreover, as will be confirmed below, low temperature chemistry plays a negligible role in propagating flames. For practical purposes, the skeletal mechanisms were further reduced for high temperature cases only, this time by including auto-ignition cases in the DRGEP process, with temperatures larger than 1000 K and a selection of 1D propagating flames for the various alkanes used for validation. The species and reactions discarded during this step constitute a low-temperature module that will be added to the kinetic scheme only when low-temperature auto-ignition characteristics are needed.

The reduction steps have been done for each mechanism, *n*-heptane and iso-octane, independently. As the goal is to derive a mechanism able to simulate PRF mixtures, the resulting skeletal mechanisms are combined. The original detailed mechanisms are very similar, as far as the base chemistry (C_1 to C_4 species) is concerned. For auto-ignition, the combined mechanism can be based on either basis chemistry, the resulting differences in the numerical solutions were found to be negligible. However, one extremely sensitive reaction for methane burning velocity has a different rate in the detailed mechanisms, namely:



In the iso-octane mechanism, the third body efficiency of this reaction is set to unity for all species, whereas in the *n*-heptane mechanism, the third-body efficiency of water is set to 12. Fig. 7(a) illustrates the effect of the definition of this reaction's third body on the burning velocity of methane. Using a large efficiency coefficient for water adds about 6 cm/s to the stoichiometric burning velocity, as compared to using a unity coefficient. In the combined mechanism, an intermediate third body has been chosen, in which water has an efficiency coefficient of 6. In the case where common reactions between the *n*-heptane and the iso-octane skeletal mechanisms have slightly different rates, the rates from the *n*-heptane mechanism are also retained. Aside from reaction (6), this choice does not affect the results.

The original detailed mechanisms from LLNL were not validated for propagating flames due to their large size. When the skeletal high temperature mechanisms for *n*-heptane and iso-octane are compared to flame experiments, a consistent trend is observed for all data at low pressure and 298 K, in which the simulated burning velocities are much higher than the experimental values. On the other hand, data at higher pressures and temperatures are either predicted correctly or slightly under-predicted by the skeletal mechanism. The strategy chosen at that point for reaching a better agreement between simulated and experimental S_u^0 at all pressures was to assume that all necessary paths were already present in the mechanism, and to update those reaction rates most sensitive to flame propagation, but fairly insensitive to homogeneous cases. The objective here was to retain the same level of accuracy for homogeneous cases as for the detailed mechanisms.

The most sensitive reactions for all alkanes involve relatively small species (up to C_4 species). The rate for the reaction



was taken from the GRI 3.0 mechanism [37]. Reaction



was taken from Dean [38]. The H abstraction by the hydrogen radical is taken from the literature review by Tsang et al. [39] for propane (reaction H237f) and from the three-parameter fit of the NIST database [40] for butane (reaction H350f). Large discrepancies are observed between experimental and simulated iso-octane burning velocities, with about 25% error overall. A limited number of reactions have been found to be sensitive for iso-octane flame propagation, but quasi-neutral in homogeneous configurations. These reactions mostly involve the iso-butenyl radical. Although new data are available for its decomposition into allene

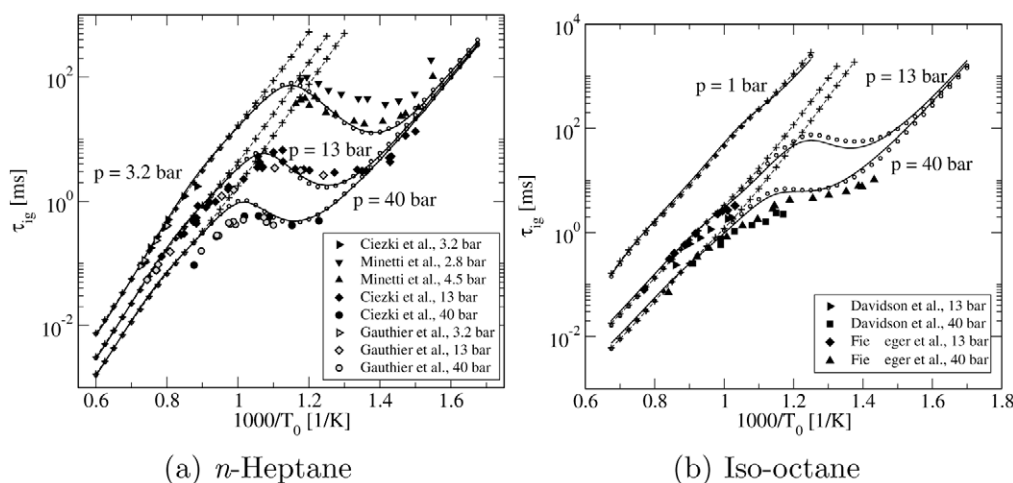


Fig. 5. Ignition delay times for stoichiometric *n*-heptane/air and iso-octane/air mixtures. Comparison between experimental data (filled symbols) and numerical results obtained using the detailed LLNL mechanisms (solid lines), the reduced combined high and low temperature mechanism (open circles), and the reduced high temperature mechanism (plus symbols, dashed lines).

Table 1

Respective sizes of the mechanisms developed in this work.

Mechanism	N_S	N_{QSS}	N_R
High temperature	99	35	669
Low temperature module	104	65	403
Combined	203	100	1071

and methyl radical (reaction H288 [41]), this new rate was not sufficient to reach a reasonable agreement with experiments and the rate of this reaction was reduced further. Rates for O and OH additions on the iso-butenyl radical (reactions H290, H291 and H376f) and H-abstraction from iso-butene (reaction H313) were also modified in order to decrease the iso-octane burning velocities.

Using the modified rates above, an extra stage of reduction is performed, including chemical lumping [42] and the introduction of quasi-steady state assumptions [36]. Two reduced sets of reactions are obtained at the end of the procedure. The first one contains all the basis chemistry and fuel decomposition reactions necessary to describe flame propagation and high temperature auto-ignition. In the following, we will refer to this set as the high temperature mechanism. The second set contains only the reactions that are important for low temperature ignition, such as molecular oxygen additions. This low temperature module is not a stand alone mechanism, and must be added to the previous set to form a combined mechanism valid for both high and low temperature ranges. The sizes of the high temperature mechanism and low temperature module are specified in Table 1. In this table, N_S is the total number of species, N_{QSS} is the number of species that can be set in steady state without introducing errors in the simulations, and N_R is the total number of reactions, with forward and backward reactions counted separately. The relatively large size of the low temperature module indicates that it should be included in the mechanism only when low temperature phenomena are of interest, and discarded otherwise.

4.1. Validation for high and low temperature auto-ignition

Figs. 5(a) and 5(b) show a comparison between experimental data and *n*-heptane and iso-octane ignition delay times obtained using the high temperature mechanism, the combined high and low temperature mechanism, and the original detailed mechanisms from LLNL. The short high temperature mechanism reproduces the ignition behavior correctly up to 1000 K, but diverts from the detailed mechanism in the NTC region, as expected. A satisfactory

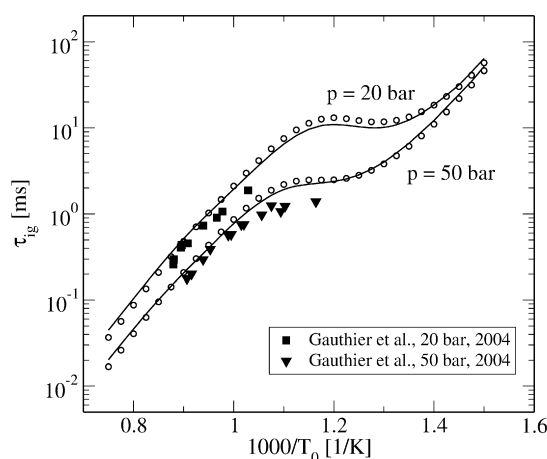


Fig. 6. Ignition delay times for stoichiometric fuel/air mixtures. Comparison between experimental data for gasoline (symbols) and numerical results for PRF 87 obtained using the detailed LLNL mechanism for PRF [20] (solid lines) and the reduced combined high and low temperature mechanism (open circles).

agreement is obtained between detailed and reduced combined high and low temperature mechanism for both *n*-heptane and iso-octane, the largest errors being obtained for iso-octane in the NTC region. Simulated ignition delay times for PRF 87 are compared with the experimental data for gasoline of Gauthier et al. [7] in Fig. 6. Although the detailed LLNL mechanism for PRF performs slightly better than the reduced scheme compared to experiments, the difference between the two mechanisms remains small. Both mechanisms predict longer ignition time than experiments, and the discrepancy can be attributed either to an inaccurate detailed chemical modeling, or an overly simplistic gasoline surrogate composition.

4.2. Validation for laminar burning velocities at low pressure

Laminar burning velocities at low pressures are computed using the reduced high temperature mechanism and compared to experimental values for methane in Fig. 7(a), ethane in Fig. 7(b), propane in Fig. 7(c), butane and iso-butane in Fig. 7(d), *n*-heptane in Fig. 8(a), iso-octane in Fig. 8(b), and PRF 85 to 95 in Fig. 8(c).

The overall agreement is very good, especially if the scatter between the various sets of experimental data is considered. It can be noted that large hydrocarbon burning velocities are under-

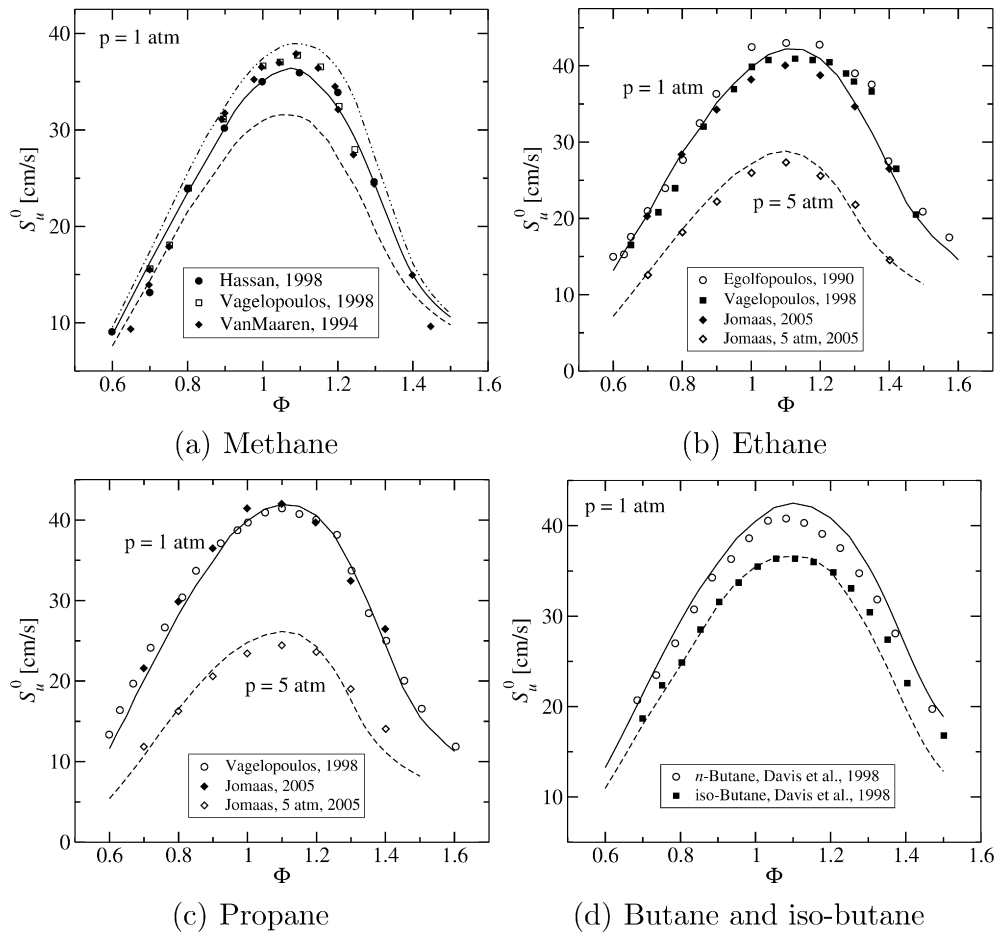


Fig. 7. Small alkane laminar burning velocities for $T_0 = 298$ K. Comparison between experimental data (symbols) and numerical results obtained using the reduced high temperature mechanism (lines). (a) illustrates the sensitivity of S_u^0 to H_2O third body efficiency in reaction H69f (=1: dashed line, =12: dash-dotted line, =6: solid line).

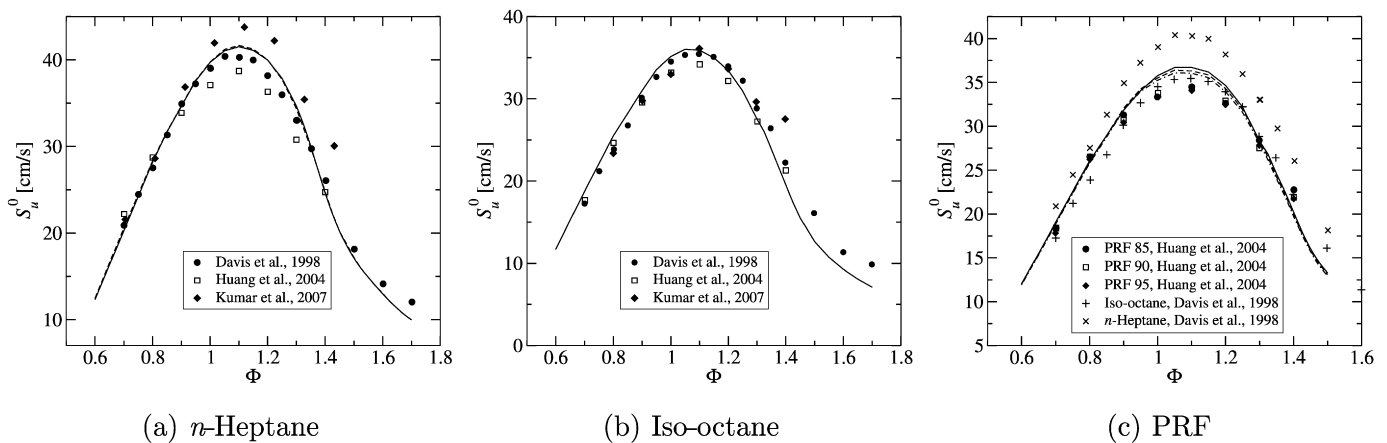


Fig. 8. Large alkane laminar burning velocities at $p = 1$ atm and $T_0 = 298$ K. Comparison between experimental data (symbols) and numerical results obtained using the reduced high temperature mechanism (lines). The dashed line in (a) is obtained using the combined high and low temperature mechanism, and illustrates the negligible role of the low temperature chemistry in flames.

predicted for rich configurations. Neither the detailed nor the reduced mechanisms contain an adequate description of the chemistry characteristic of rich oxidation, such as the formation of polycyclic aromatic hydrocarbons, which might explain the observed discrepancy. Also, it might appear that the laminar burning velocities of PRF mixtures are over-predicted when compared to the experimental data from Huang et al. [13]. However, the experimental data from the same group for *n*-heptane and iso-octane

are lower than other reported datasets, for example by Davis and Law [12]. For reference, the laminar burning velocities for pure *n*-heptane and iso-octane from Davis and Law have been added in Fig. 8(c), and the simulated burning velocities for PRF are standing, as expected, between the lower values of pure iso-octane and the higher values of pure *n*-heptane. Finally, a comparison between the laminar burning velocities of *n*-heptane when using the high temperature mechanism or the combined high and low temper-

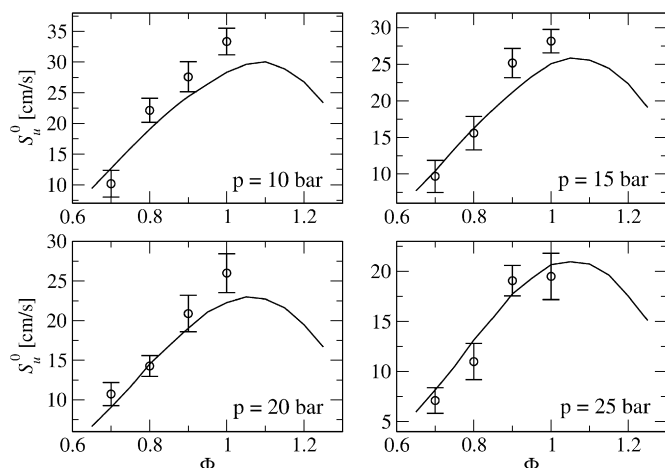


Fig. 9. Laminar burning velocities of *n*-heptane/air ($X_{O_2}^{air} = 0.205$) mixtures at high pressures and $T_0 = 373$ K. Comparison between experimental data obtained in this work (symbols) and numerical results obtained using the reduced high temperature mechanism (solid lines).

ature mechanism is shown in Fig. 8(a). The negligible difference between the results confirms that low temperature chemical pathways play no role in propagating flames.

5. Results

The results for the measured unburned unstretched laminar flame velocities are summarized and discussed in the present section. Results are given in Fig. 9 for *n*-heptane/air mixtures, in Fig. 10 for iso-octane/air mixtures, and in Fig. 11 for PRF 87 and standard gasoline/air mixtures. At least three distinct experiments were conducted for each set of initial conditions. The different measurements were then used to estimate the standard deviation for each condition. Error bars reflecting these standard deviations are shown in Figs. 9 to 13. To widen the scope of the comparison, experimental data taken from related literature have been added, including the data from Bradley et al. [15] for iso-octane/air mixtures at $p = 10$ bar and $T_0 = 358$ K, as well as the extrapolated data by Metghalchi and Keck [16], and data by Gülder [17] at $T_0 = 373$ K. Surprisingly, Gülder's laminar burning velocities at high pressures differ to a great extent from the other sets of experiments and are even higher than data at atmospheric pressure. A possible explanation may be found in the technique used to measure the growth rate of the spherical flame inside the vessel. Indeed, Gülder used six ionization probes whereas the more recent works use an optical Schlieren measurement technique combined with a high speed camera to track the expanding flame front. Furthermore, Gülder did not correct his measured flame propagation results to zero stretch. The data of Metghalchi and Keck [16] are slightly higher than the measured and calculated data for iso-octane/air mixtures from this work, while data from Bradley et al. [15] at 10 bar initial pressure are in excellent agreement with the present work, considering the small differences in initial temperature between both works.

Essentially, all results measured in this work show an increase in the laminar burning velocity for lean up to slightly rich conditions, while the burning velocity decreases for even richer mixtures. The error bars of all investigated laminar burning velocities are slightly increasing when increasing the initial pressure. This can be observed by comparing the error bars at 10 and 25 bar in Figs. 9 to 11. Nonetheless each error bar was determined from three investigated results of the laminar burning velocity. Therefore fluctuations in the accuracy of the standard deviation could

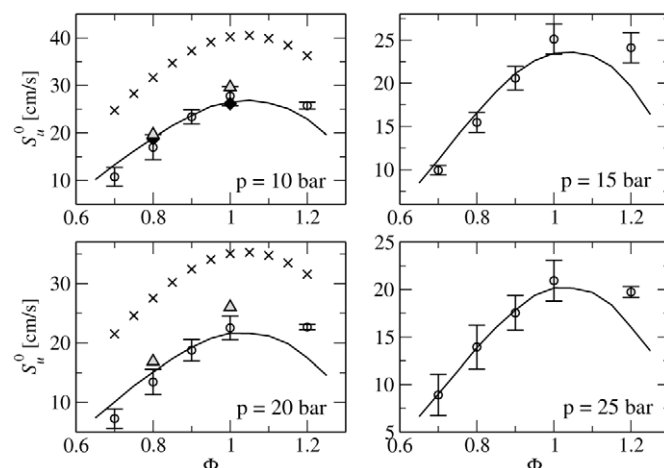


Fig. 10. Laminar burning velocities of iso-octane/air ($X_{O_2}^{air} = 0.205$) mixtures at high pressures. Comparison between experimental data at $T_0 = 373$ K obtained in this work (circles), numerical results obtained using the reduced high temperature mechanism (solid lines), data from Bradley et al. [15] at $T_0 = 358$ K (filled diamonds), data extrapolated at $p = 10$ and 20 bar and $T_0 = 373$ K from Metghalchi and Keck [16] (triangles), and data by Gülder [17] at $T_0 = 373$ K (crosses).

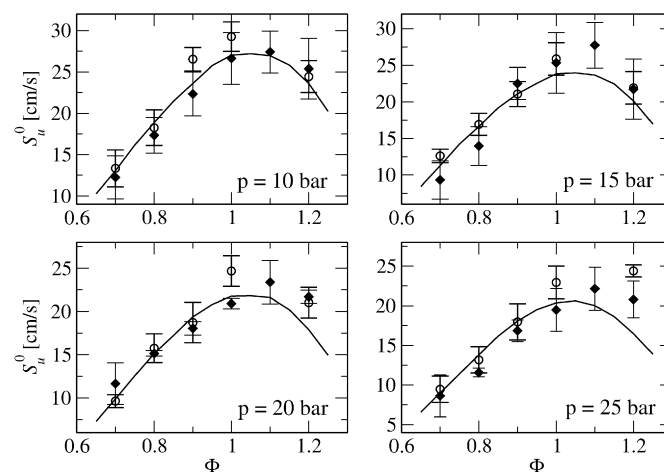


Fig. 11. Laminar burning velocities of PRF/air ($X_{O_2}^{air} = 0.205$) mixtures at high pressures and $T_0 = 373$ K. Comparison between experimental data obtained in this work for PRF 87 (open circles) and gasoline (filled diamonds), and numerical results obtained using the reduced high temperature mechanism for PRF 87 (solid lines).

occur, but still not affect the accuracy of the absolute value of the results.

To analyze the observed flame data, only information of smoothly propagating flames was used to determine the laminar burning velocity and Markstein numbers of the investigated mixtures. This is of particular importance, because for rich mixtures, the Lewis number of the deficient component (oxygen) of the mixture decreases, therefore the mass transport due to diffusivity becomes dominant due to the heat diffusivity. Thermodynamic instabilities start to occur at a certain flame radius due to a critical Peclet number, and the development of wrinkles can be observed. From that point on the flame speed increases rapidly. Data from that regime cannot be used for flame analysis. However, even the rich flames investigated in the present work provided sufficient data for an accurate analysis of the investigated quantities.

The predicted laminar burning velocities for *n*-heptane/air mixtures close to stoichiometry are lower than the experimental results for pressures up to 20 bar, whereas for lean conditions or at higher pressure, a very good agreement between experimental and numerical results can be observed. For the measured iso-octane/air

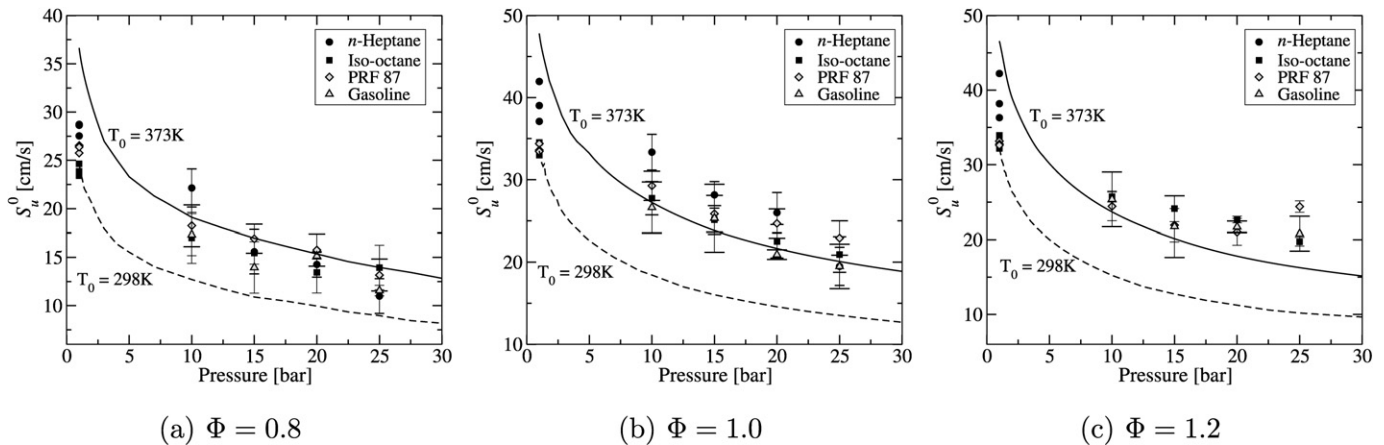


Fig. 12. Pressure dependency of laminar burning velocities. Comparison between experimental data (symbols) and numerical results obtained using the reduced high temperature mechanism for PRF 87 (lines). Data at 1 bar are obtained with $T_0 = 298$ K (simulation: dashed line), data at higher pressures are obtained with $T_0 = 373$ K (simulation: solid line).

cases for lean up to stoichiometric mixtures, the results show excellent agreement with the modeled burning velocities. The measured data of Metghalchi and Keck [16], Bradley et al. [15], and the data measured in this work essentially agree well with the numerical results. However, for rich cases, the simulated values tend to have a stronger equivalence ratio dependence compared to the experiments. As mentioned before, a possible explanation may be the inadequate representation of rich hydrocarbon oxidation, from soot precursors to PAHs formation.

Primary Reference Fuel, which consists of 87% iso-octane and 13% *n*-heptane by liquid volume at ambient condition, as well as standard gasoline (octane number 90) for automotive engines, were also investigated focussing on the determination of laminar burning velocities and Markstein lengths. Fig. 11 shows experimental as well as numerical results for PRF 87/air and gasoline/air mixtures from 10 bar up to 25 bar at 373 K initial pressure. Laminar burning velocities for both PRF 87/air mixtures and real gasoline/air mixtures are in good agreement for lean mixtures up to stoichiometric conditions, for which the computed values for the PRF 87/air mixtures are approximately 10–15% lower than the experimental data.

The comparison of the burning velocities of the different fuels shows that PRF 87 appears to be a valuable surrogate for gasoline with similar properties at all pressures. For a better understanding of the pressure dependence with respect to the laminar burning velocity, a comparison is shown in Fig. 12. For the lean and stoichiometric mixtures, S_u^0 is a monotonically decreasing function of the pressure, well reproduced by the kinetic mechanism. As discussed earlier, for the rich cases, the computed burning velocities are lower than those from the experiments, which reach an almost constant value for higher pressures.

As dilution of combustible mixtures is important for combustion in automotive engines, especially for EGR (Exhaust Gas Recirculation), laminar burning velocity measurements for diluted gasoline/air mixtures were also conducted. There are several reasons to dilute combustible mixtures for automotive engines, most importantly the reduction of burnt gas temperatures to reduce the emissions of oxides of nitrogen. In this work, standard gasoline/air mixtures are diluted with pure nitrogen, which is used as a surrogate for engine exhaust gas. The data experimentally obtained for diluted gasoline/air mixtures are compared with computational results for the PRF 87 surrogate. Results for two different diluted mixtures are presented in Fig. 13. The first mixture uses an oxidizer composed of 15% oxygen and 85% nitrogen, the second one uses an oxidizer composed of 17% oxygen and 83% nitrogen. Both experimental and numerical results show a strong dependence of

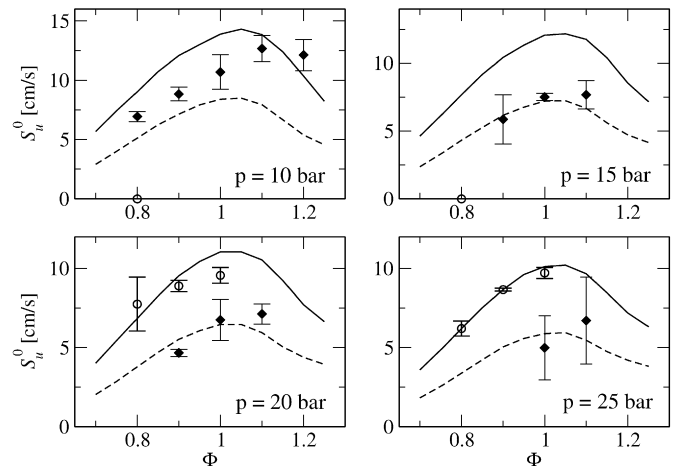


Fig. 13. Laminar burning velocities of diluted fuel/air mixtures at high pressures and $T_0 = 373$ K. Comparison between experimental data for gasoline obtained in this work ($X_{O_2}^{air} = 0.17$: open circles, $X_{O_2}^{air} = 0.15$: filled diamonds) and numerical results obtained using the reduced high temperature mechanism for PRF 87 ($X_{O_2}^{air} = 0.17$: solid lines, $X_{O_2}^{air} = 0.15$: dashed lines).

the laminar burning velocities on the level of dilution of the mixtures. The numerical results agree reasonably well for the 17% oxygen case. For the 15% oxygen case, the predicted burning velocities are approximately 20–25% higher than the experimental data for the 10 bar case. For higher pressures, the agreement is quite good.

Finally, burned gas Markstein numbers for the low and the high pressure cases were determined for all investigated fuel/air mixtures. Results are shown in Fig. 14, where in addition Markstein numbers for iso-octane/air mixtures obtained from the theory of Bechtold and Matalon [43] are shown. The theory for predicting the corresponding Markstein numbers is based on a one step reaction scheme that assumes large activation energies. Therefore, discrepancies between experimentally and numerically determined quantities can occur. Bechtold and Matalon [43] showed that the theory applied to iso-octane/air mixtures at ambient conditions yields satisfactory results. Therefore, the theory was also applied for the conditions studied in this work and compared to the experimental results. For both high and low pressure cases, the Markstein numbers decrease with increasing equivalence ratio. The data agree qualitatively with the theoretical predictions. It is interesting to note that the Markstein numbers for *n*-heptane/air and gasoline/air mixtures at the lower pressure are approximately twice

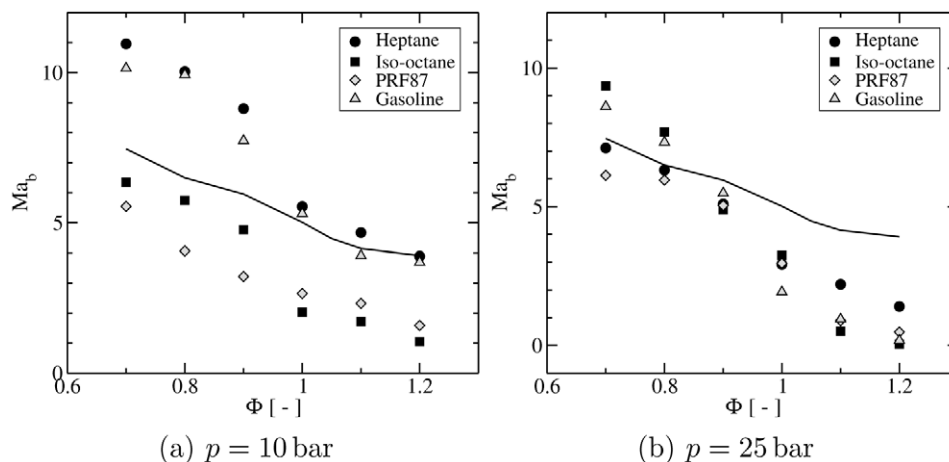


Fig. 14. Burned Markstein numbers for *n*-heptane, iso-octane, PRF 87 and gasoline/air ($X_{O_2}^{air} = 0.205$) mixtures at high pressures and $T_0 = 373$ K. Comparison between experimental data obtained in this work (symbols) and theoretical predictions from Bechtold and Matalon [43] (solid lines).

higher than those determined for iso-octane/air and PRF 87/air mixtures, while at higher pressure, the difference is smaller. As already mentioned above, the theory definitely has limitations. Nonetheless, a good qualitative agreement between experimental and numerical results is shown. For a further quantitative analysis however, the theory needs to be revised.

6. Conclusion

Laminar burning velocities and Markstein numbers have been experimentally determined for *n*-heptane, iso-octane, PRF 87, and gasoline/air mixtures at engine-relevant conditions, and were compared with existing experimental data. A reduced kinetic mechanism derived from the Lawrence Livermore detailed *n*-heptane and iso-octane mechanism was validated for both homogeneous systems and for propagating flames. Satisfactory agreement was obtained between the new high pressure burning velocity measurements and predictions using the reduced mechanism. The experimentally determined burned gas Markstein numbers Ma_b were in a reasonable agreement with theoretical calculations.

References

- [1] N. Peters, Fifteen Lectures on Laminar and Turbulent Combustion, ERCOFTAC Summer School (1992), <http://www.itv.rwth-aachen.de/Downloadarea/Summerschool92>.
- [2] J. Ewald, N. Peters, Proc. Combust. Inst. 31 (2007) 3051–3058.
- [3] C. Baumgarten, Mixture Formation in Internal Combustion Engines, Springer, Berlin/Heidelberg/New York, 2006.
- [4] D.J. Cook, H. Pitsch, J.H. Chen, E.R. Hawkes, Proc. Combust. Inst. 31 (2007) 2903–2911.
- [5] W.J. Pitz, N.P. Cernansky, F.L. Dryer, F.N. Egolfopoulos, J.T. Farrell, D.G. Friend, H. Pitsch, SAE 2007-01-0175 (2007).
- [6] H.K. Ciezki, G. Adomeit, Combust. Flame 93 (1993) 421–433.
- [7] B.M. Gauthier, D.F. Davidson, R.K. Hanson, Combust. Flame 139 (2004) 300–311.
- [8] R. Minetti, M. Carlier, M. Ribaucour, E. Therssen, L.R. Sochet, Combust. Flame 102 (1995) 298–309.
- [9] K. Fieweger, R. Blumenthal, G. Adomeit, Combust. Flame 109 (1997) 599–619.
- [10] C.V. Callahan, T.J. Held, F.L. Dryer, R. Minetti, M. Ribaucour, L.R. Sochet, T. Faravelli, P. Gaffuri, E. Ranzi, Proc. Combust. Inst. 26 (1996) 739–746.
- [11] D. Davidson, B. Gauthier, R. Hanson, Proc. Combust. Inst. 30 (2005) 1175–1182.
- [12] S.G. Davis, C.K. Law, Combust. Sci. Technol. 140 (1998) 427–450.
- [13] Y. Huang, C.J. Sung, J.A. Eng, Combust. Flame 139 (2004) 239–251.
- [14] K. Kumar, J.E. Freeh, C.J. Sung, Y. Huang, J. Prop. Power 23 (2007) 428–436.
- [15] D. Bradley, R.A. Hicks, R.A. Lawes, C. Sheppard, R. Wolley, Combust. Flame 115 (1998) 126–144.
- [16] M. Metghalchi, J.C. Keck, Combust. Flame 48 (1982) 191–210.
- [17] O.L. Gülder, SAE 841000 (1984).
- [18] H.J. Curran, P. Gaffuri, W.J. Pitz, C.K. Westbrook, Combust. Flame 114 (1998) 149–177.
- [19] H.J. Curran, P. Gaffuri, W.J. Pitz, C.K. Westbrook, Combust. Flame 129 (2002) 253–280.
- [20] H.J. Curran, W.J. Pitz, C.K. Westbrook, C.V. Callahan, F.L. Dryer, Proc. Combust. Inst. 27 (1998) 379–387.
- [21] M. Chaos, A. Kazakov, Z. Zhao, F.L. Dryer, Int. J. Chem. Kinet. 39 (2007) 399–414.
- [22] <http://www.stanford.edu/group/pitsch/ces.htm>.
- [23] J. Warnatz, U. Maas, R.W. Dibble, Combustion: Physical and Chemical Fundamentals, Modeling and Simulation, Experiments, Pollutant Formation, Springer, Berlin, 2006.
- [24] G. Rozenchan, D. Zhu, C. Law, S. Tse, Proc. Combust. Inst. 29 (2002) 1461–1469.
- [25] N. Peters, Turbulent Combustion, Cambridge University Press, Cambridge, 2000.
- [26] G. Rozenchan, S. Tse, D. Zhu, C. Law, Laminar Burning Rates and Markstein Length of CH_4/O_2 Inert Mixtures at High Pressures, in: 39th Aerospace Sciences Meeting & Exhibit, AIAA (2001).
- [27] D.R. Dowdy, D.B. Smith, S.C. Taylor, A. Williams, Combust. Symp. 23 (1990) 325–332.
- [28] F.A. Williams, Combustion Theory, Addison–Wesley, Menlo Park, CA, 1985.
- [29] H. Pitsch, FlameMaster, a C++ computer program for 0D combustion and 1D laminar flame calculations.
- [30] P. Ronney, in: H.D. Ross (Ed.), Microgravity Combustion: Fire in Free, Academic Press, 2001, Chapter 2, pp. 299–418.
- [31] A. Van Maaren, D.S. Thung, L.P.H. De Goeij, Combust. Sci. Technol. 96 (1994) 327–344.
- [32] M.I. Hassan, K.T. Aung, G. Faeth, Combust. Flame 115 (1998) 539–550.
- [33] C.M. Vagelopoulos, F.N. Egolfopoulos, Proc. Combust. Inst. 27 (1998) 513–520.
- [34] F. Egolfopoulos, D. Zhu, C. Law, Proc. Combust. Inst. (1991) 471–478.
- [35] G. Jomaas, X. Zheng, D.L. Zhu, C.K. Law, Proc. Combust. Inst. 30 (2005) 193–200.
- [36] P. Pepiot-Desjardins, H. Pitsch, Combust. Flame 154 (2008) 67–81.
- [37] G. Smith, D. Golden, M. Frenklach, N. Moriarty, B. Eiteneer, M. Goldenberg, C. Bowman, R. Hanson, S. Song, W. Gardiner, V. Lissianski, Z. Qin, http://www.me.berkeley.edu/gri_mech/.
- [38] A.M. Dean, J. Phys. Chem. 89 (1985) 4600–4608.
- [39] B.V. Buxton, C.L. Greenstock, W.P. Helman, A.B. Ross, W. Tsang, J. Phys. Chem. Ref. Data 17 (1988) 513–886.
- [40] <http://kinetics.nist.gov/>.
- [41] X.L. Zheng, H.Y. Sun, C.K. Law, J. Phys. Chem. A 109 (2005) 9044–9053.
- [42] P. Pepiot-Desjardins, H. Pitsch, Combust. Theory Model. (2008), in press.
- [43] J.K. Bechtold, M. Matalon, Combust. Flame 127 (2001) 1906–1913.